Journal of Applied Physics ARTICLE pubs.aip.org/aip/jap

Extracting surface and bulk recombination parameters for passivated silicon using photoexcited muon spin spectroscopy

Cite as: J. Appl. Phys. **138**, 135701 (2025); doi: 10.1063/5.0288808
Submitted: 24 August 2025 · Accepted: 14 September 2025 ·
Published Online: 1 October 2025

View Online Export Citation CrossMark

Anup Yadav,[1] Sophie L. Pain,[1] Luke Wilkins,[1] Nicholas E. Grant,[1] James S. Lord,[2] Koji Yokoyama,[2] and John D. Murphy[1,3,a)]

AFFILIATIONS

[1]School of Engineering, University of Warwick, Coventry CV4 7AL, United Kingdom
[2]ISIS Neutron and Muon Source, STFC Rutherford Appleton Laboratory, Didcot OX11 0QX, United Kingdom
[3]School of Engineering, University of Birmingham, Edgbaston, Birmingham B15 2TT, United Kingdom

[a)]**Author to whom correspondence should be addressed:** j.d.murphy@bham.ac.uk

ABSTRACT

Photoexcited muon spin spectroscopy (photo-μSR) enables depth-resolved measurement of charge carrier lifetimes in semiconductors. In this work, we evaluate the sensitivity of photo-μSR to surface recombination by studying silicon wafers with asymmetric surface passivation. One surface has a surface recombination velocity (SRV) of ∼1 cm/s while the other has an SRV in the range ∼1–10 000 cm/s. Charge carriers are generated using 1064 nm laser excitation and the resulting depth-dependent carrier profiles are modeled using a 1D diffusion equation. By comparing depth-resolved photo-μSR carrier lifetime spectra to simulations, we extract bulk carrier lifetime, which we benchmark against values obtained from photoconductance decay (PCD). With knowledge of the bulk carrier lifetime, we then perform further simulations to extract SRV values. The study demonstrates that photo-μSR can resolve differences in surface passivation quality across a broad range (∼10–5000 cm/s) of SRVs. These findings establish photo-μSR as a powerful tool and complementary method to PCD measurements for disentangling surface and bulk recombination in semiconductor materials and devices.

I. INTRODUCTION

Minority charge carrier lifetime determines the performance of certain electronic devices, such as silicon solar cells. Charge carrier recombination occurs through Shockley–Read–Hall (SRH), radiative, and Auger mechanisms in the bulk and also via surface-related processes. High-quality silicon has relatively little SRH recombination and, under moderate or low carrier injection when Auger recombination is weak, effective excess charge carrier lifetime (τ_{eff}) is often limited by surface recombination. Surface passivation—often achieved by the deposition of dielectric thin films—enhances τ_{eff}.

Surface recombination velocity (SRV) is used to quantify surface passivation quality. For a symmetrically passivated bulk semiconductor sample, τ_{eff} relates to bulk excess charge carrier lifetime (τ_{bulk}) and SRV according to[1]

$$\frac{1}{\tau_{\text{eff}}} = \frac{1}{\tau_{\text{bulk}}} + \frac{2\text{SRV}}{d}, \tag{1}$$

where d is its thickness. Accurate determination of SRV requires knowledge of the bulk lifetime (τ_{bulk}), else SRV values should be considered upper limits, with the limitations of Eq. (1) discussed elsewhere.[1] Conventional photoconductance decay (PCD) measurements of τ_{eff} are unable to separate surface and bulk effects unambiguously from a single sample. To achieve this, we employ photoexcited muon spin spectroscopy (photo-μSR) as a depth-resolved pump–probe technique for studying charge carrier dynamics.[2] In photo-μSR, excess charge carriers are generated by a

laser pulse followed by implantation of ∼4 MeV spin-polarized positive muons (μ^+). These positive muons capture electrons to form hydrogen-like muonium "atoms" which undergo a series of reactions, resulting in spin depolarization.[3–7] The muon spin asymmetry is determined from detection of positrons emitted upon μ^+ decay, and its relaxation rate directly correlates with the excess carrier density (Δn).[2] Photo-μSR offers advantages over PCD as it can measure carrier lifetime: (i) as a function of depth by adjusting the muon implantation position[8,9] and (ii) in completed devices such as silicon photovoltaic cells.[9]

Photo-μSR's ability to separate bulk and surface recombination has been shown in principle, but only on poorly passivated chemically treated silicon wafers (SRV > 100 cm/s), without validatory PCD measurements.[8] Here, we apply photo-μSR to a broader range of passivation schemes, including state-of-the-art dielectric films grown by atomic layer deposition (ALD), with PCD validation on the same samples. To interpret depth-dependent photo-μSR data, we develop a 1D charge carrier diffusion model that simulates the excess carrier profile generated by 1064 nm laser illumination, enabling estimation of τ_{bulk} and *SRV* from a single sample.

II. EXPERIMENTAL METHODS

$5 \times 5\ cm^2$ samples were studied and cut from 900 μm thick, boron-doped *p*-type ∼5 Ω cm Czochralski silicon wafers. Muon irradiation can introduce recombination-active defects leading to degradation of bulk carrier lifetime.[9,10] Low bulk carrier lifetime (∼1 ms at $\Delta n = 1 \times 10^{15}\ cm^{-3}$) wafers were selected to reduce the relative impact of muon-induced defects. Following thorough chemical cleaning,[11] plasma-enhanced atomic layer deposition (PE-ALD)[12] in a Veeco Fiji G2 system was used to deposit films at 200 °C, with parameters published previously.[13] For all samples, one surface was coated with ∼20 nm Al_2O_3 providing excellent passivation (SRV <1 cm/s).[14,15] The other surface was either left uncoated or coated by ALD with ∼20 nm Al_2O_3, HfO_2, or SiO_2. ALD of Al_2O_3 and SiO_2 involved an O_2-plasma co-reactant, while ALD of HfO_2 involved an O_3 co-reactant. All samples were annealed for 30 min in air in a quartz tube furnace at ∼450 °C to "activate" the passivation.[15,16] Exposure of the uncoated surface to atmosphere resulted in the formation of an ultra-thin (∼1 nm) "native" oxide layer.[17] Effective carrier lifetimes were measured by PCD (denoted as τ_{PCD}) prior to and after muon exposure using a Sinton WCT-120 lifetime tester (software version v5.74).

Photo-μSR was performed in the high magnetic field muon spectrometer (HiFi) at ISIS Neutron and Muon Source at the STFC Rutherford Appleton Laboratory.[18] Samples were mounted onto an aluminum sample holder with silicone vacuum grease and were held at 305 K using a closed cycle refrigerator. The measurement setup is illustrated schematically in Fig. 1(a). A 100% spin-polarized 3.8 MeV μ^+ pulse at 50 Hz was directed onto the side of the samples on which SRV was intentionally varied. A Nd:YAG laser illuminated the Al_2O_3-passivated surface with 1064 nm pulses with an energy of ∼0.03 mJ/pulse at a repetition rate of 25 Hz with a circular beam area of $\sim 10\ cm^2$. Since the laser spot was significantly larger than the circular muon beam area ($\sim 2\ cm^2$), the region probed by muons is assumed to experience uniform carrier generation. The diffusion length of the photoexcited carriers lies well within the illuminated region meaning lateral diffusion effects can be neglected. To decouple muon spin relaxation (μSR) caused by photoexcited charge carriers from intrinsic μSR without illumination (i.e., dark-μSR), a longitudinal magnetic field (5 mT) was applied parallel to the initial muon spin direction (opposite to the muon momentum). This field suppresses intrinsic μSR due to slowly fluctuating local magnetic fields, thereby enhancing measurement sensitivity to μSR induced by photoexcited charge carriers.[19] The time evolution of the μSR was recorded as a function of time delay between the muon and the laser pulse (Δt).

Figure 1(b) presents the light absorption profile and simulated muon distributions. The former was calculated by determining incident photon flux, considering laser power, laser beam area, and photon energy. Photon absorption was estimated using silicon's absorption coefficient, a_λ ($\sim 10\ cm^{-1}$ for 1064 nm excitation[20]), and the Beer–Lambert law. Muons were implanted at three distinct depths (denoted Depths 1, 2, and 3 in order of increasing depth). Depth 3 was achieved with a directly incident muon beam. Depths 1 and 2 were obtained by placing respective 448 and 224 μm thick aluminum degraders into the muon path. Muon distributions were simulated using Monte Carlo packages "musrSim" and "musrSimAna,"[21] based on Geant4. Each depth has ∼140 μm full width at half maximum. Table I summarizes muon exposure conditions, with implantation events estimated from scintillator detector count rates.

The variation of Δn with Δt is shown in a photo-μSR carrier lifetime spectrum (CLS), generated as described previously.[2,8] Data were collected under both dark and illuminated conditions, with muon spin relaxation rates (λ) measured as a function of Δn. An example asymmetry spectrum for $Al_2O_3/Si/Al_2O_3$ is shown in Fig. 1(c). Asymmetry spectra collected under illumination were fitted with a single exponential decay function over a defined time range (0.1–0.5 μs) to extract the corresponding λ.[2] Δn values were calibrated by adjusting laser power with neutral density filters, with resulting λ values fitted to a power law $[\lambda = \beta(\Delta n/\Delta n_0)^\alpha]$ to derive a calibration curve, as shown in Fig. 1(d), which provides a relationship between λ and Δn. For each sample, a calibration curve was obtained at Depth 3 at which all the muons were implanted within the sample. This curve was subsequently used to convert λ values at other depths into corresponding Δn values, enabling a CLS to be constructed.

III. RESULTS AND DISCUSSION

All samples were characterized via PCD to assess their passivation level prior to photo-μSR. We fabricated control samples with identical dielectric layers on both surfaces (i.e., $Al_2O_3/Si/Al_2O_3$, $HfO_2/Si/HfO_2$, $SiO_x/Si/SiO_x$, and native SiO_x/Si/native SiO_x) to extract upper-limit SRV values using Eq. (1). We take τ_{bulk} as the intrinsic lifetime limit,[22] but this is conservative due to bulk SRH recombination. Figure 2(a) presents the upper-limit SRV values extracted as a function of Δn. At $\Delta n = 1 \times 10^{14}\ cm^{-3}$ (similar to in photo-μSR), the upper-limit SRVs are ∼20, 42, and 10^4 cm/s for Al_2O_3, HfO_2, and SiO_x passivation, respectively. The SRV of native SiO_x/Si/native SiO_x at this injection level could not be reliably extracted due to low PCD signal. The inferred upper-limit SRVs for the *p*-type silicon wafers used are significantly higher than those previously achieved with similar dielectric layers on *n*-type

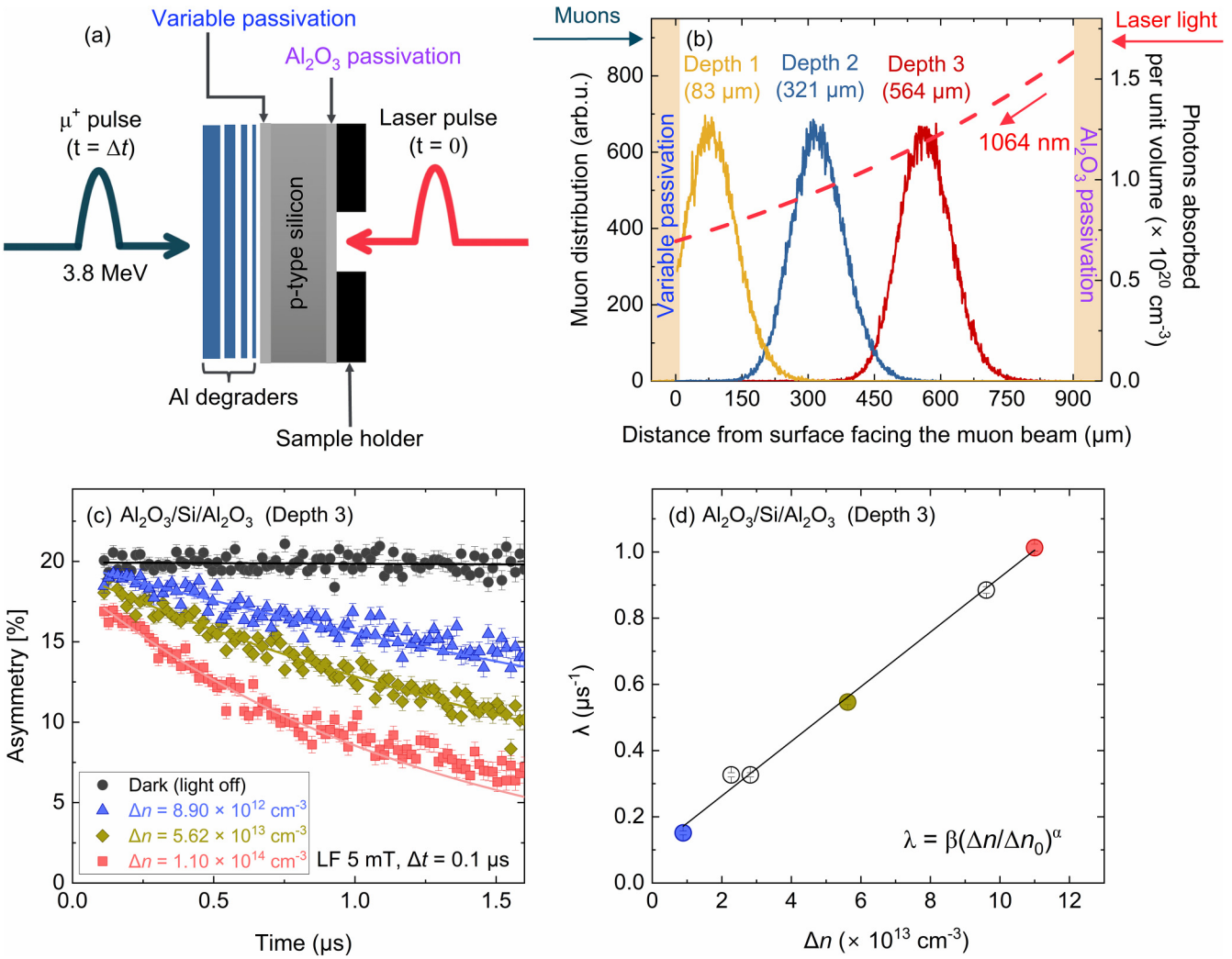

FIG. 1. (a) Configuration of the photo-μSR experiment. (b) Muon depth profile (left axis) and photon absorption profile (right axis). (c) Representative μSR asymmetry-time data for light "off" and light "on" conditions for different Δn levels at Depth 3 under longitudinal field (LF) of 5 mT. Time on the horizontal axis is that since the muon pulse. Each data set in (c) corresponds to 15×10^6 events. (d) Muon spin relaxation rate (λ) vs Δn, with the fit giving $\alpha = 0.84$, $\beta = 0.94\,\mu s^{-1}$, and $\Delta n_0 = 1.1 \times 10^{14}$ cm^{-3}. Data in (c) and (d) are for the $Al_2O_3/Si/Al_2O_3$ sample.

substrates (i.e., <1, ~11, and >700 cm/s for Al_2O_3,[15] HfO_2,[23] and SiO_x,[13] respectively, grown under these conditions via ALD and >4000 cm/s for SiO_x grown in air[17]). The higher upper-limit SRVs in *p*-type substrates reflect the greater bulk recombination compared to *n*-type substrates, while the shorter bulk carrier lifetime *p*-type substrates make them less sensitive to muon beam-induced carrier lifetime degradation.

Figures 2(b) and 2(c) show effective lifetime curves for asymmetrically passivated samples along with symmetrically passivated $Al_2O_3/Si/Al_2O_3$. Differences in passivation achieved by different dielectric layers are evident. $Al_2O_3/Si/Al_2O_3$ and $HfO_2/Si/Al_2O_3$ show the highest effective lifetimes—due to both-sided good passivation—while $SiO_x/Si/Al_2O_3$ and native $SiO_x/Si/Al_2O_3$ exhibit significantly shorter effective lifetimes because of worse passivation on one side. Figure 2(b) corresponds to carrier lifetime measured with illumination from the variable passivation surface, whereas Fig. 2(c) shows data with illumination from the Al_2O_3-passivated surface. The latter is substantially higher for $SiO_x/Si/Al_2O_3$ and native $SiO_x/Si/Al_2O_3$, because carriers are generated nearer to the well-passivated surface and can diffuse further.

To extract SRV values from experimentally determined photo-μSR CLS, we apply a 1D carrier diffusion model. The model relies on solutions to the 1D diffusion equation for the excess carrier density accounting for carrier diffusion and

TABLE I. Muon exposure conditions.

Sample structure	Dielectric on muon-incident surface	Muon exposure duration (h)	Estimated total muon dose (millions of events)
$Al_2O_3/Si/Al_2O_3$	Al_2O_3	30.5	1410
$HfO_2/Si/Al_2O_3$	HfO_2	27.0	1350
$SiO_x/Si/Al_2O_3$	SiO_x	23.5	1365
Native $SiO_x/Si/Al_2O_3$	Native SiO_x	27.5	1540

recombination,[24]

$$\frac{\partial \Delta n(z,t)}{\partial t} = D_a \frac{\partial^2 \Delta n(z,t)}{\partial z^2} - \frac{\Delta n(z,t)}{\tau_{bulk}}, \quad (2)$$

where D_a is the ambipolar diffusion coefficient of charge carriers in silicon (32 cm^2/s[24]), z represents position along the muon/laser axis, and t is the time. Muons were incident at $z = 0$, while laser illumination occurs at the opposite surface at $z = d$. To solve Eq. (2), numerical integration was performed using Lax–Friedrich's finite difference method with time step $dt = 1$ ns and the wafer divided into cells of width $dz = 5\,\mu$m, following a previous approach.[8] PC1D software[25] was used to simulate the variations in Δn as a function of depth within the silicon wafer. These simulated curves were then compared with Δn profiles generated by the 1D model to benchmark and validate its accuracy. Boundary conditions were imposed to decouple τ_{bulk} and SRV. On the laser-illuminated surface,

$$\Delta n(d, t + dt) = \Delta n(d, t) e^{-\mathrm{SRV}_{laser}\frac{dt}{dz}}, \quad (3)$$

where SRV_{laser} represents the SRV on the laser-incident surface, which was set to 1 cm/s such that Δn decreases by $e^{-\mathrm{SRV}_{laser}\,dt/dz}$ with each time step. On the muon-incident surface,

$$\Delta n(0, t + dt) = \Delta n(0, t) e^{-\mathrm{SRV}_{muon}\frac{dt}{dz}}, \quad (4)$$

where SRV_{muon} refers to SRV on the muon-incident surface and was varied from 1 to 10 000 cm/s. To account for differences in amplitude between experimental and simulated data, a scaling factor (0–1) was applied to each simulated curve for each muon implantation depth. Such scaling does not affect the shape or the decay rate.

Extracting SRV requires knowledge of τ_{bulk}, which we estimate using superacid re-passivation with bis(trifluoromethanesulfonyl)amide ("TFSA") in pentane. This is a highly effective temporary surface passivation technique (SRV < 1 cm/s[11,26]), which does not impact bulk carrier lifetime. Figure 3(a) shows PCD measurements for two samples, both previously symmetrically passivated with Al_2O_3, following superacid passivation. One had been exposed to muons, while the other control sample had not. The muon-irradiated sample exhibits shorter carrier lifetime due to muon-induced bulk defects.[9,10] As superacid passivation provides highly effective surface passivation,[15] τ_{PCD} is indicative of τ_{bulk}.

To validate PCD-inferred τ_{bulk}, we measured the photo-μSR CLS at Depth 3 (564 μm) for $Al_2O_3/Si/Al_2O_3$ and compared it to curves simulated for various bulk carrier lifetimes (τ_{bulk} = 50–350 μs), assuming excellent surface passivation (SRV = 1 cm/s on both surfaces). As shown in Fig. 3(b), the best agreement between simulation and experiment was achieved for $\tau_{bulk} \sim 150\,\mu$s at $\Delta n = 1 \times 10^{14}\,cm^{-3}$, consistent with PCD results shown in Fig. 3(a). We, therefore, fixed $\tau_{bulk} = 150\,\mu$s in simulations for asymmetrically passivated samples.

Asymmetrically passivated samples were used to understand passivation by other dielectrics. Figure 4 presents photo-μSR CLS at three depths for three samples: $HfO_2/Si/Al_2O_3$, $SiO_x/Si/Al_2O_3$, and native $SiO_x/Si/Al_2O_3$. Curves in Fig. 4 are from the 1D

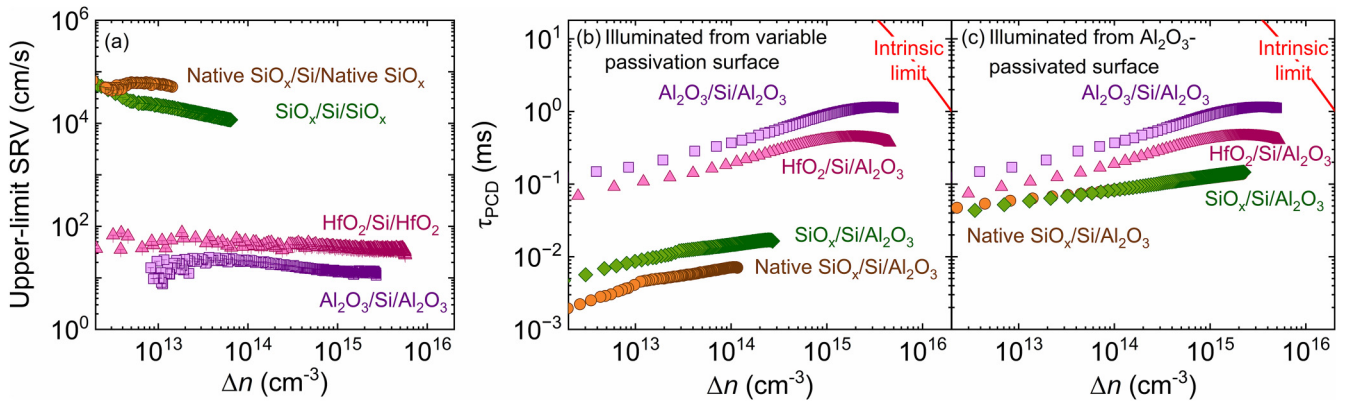

FIG. 2. PCD measurements prior to muon exposure performed using generalized (1/1) mode (which includes both transient and quasi-steady-state PCD). (a) Upper-limit SRVs extracted using Eq. (1) for symmetrically passivated samples. (b) and (c) Injection-dependent effective carrier lifetime for $Al_2O_3/Si/Al_2O_3$, $HfO_2/Si/Al_2O_3$, $SiO_x/Si/Al_2O_3$, and native $SiO_x/Si/Al_2O_3$. Measurements were made with samples illuminated from the (b) variable passivation surface or (c) Al_2O_3-passivated surface. The intrinsic lifetime limit[22] is shown.

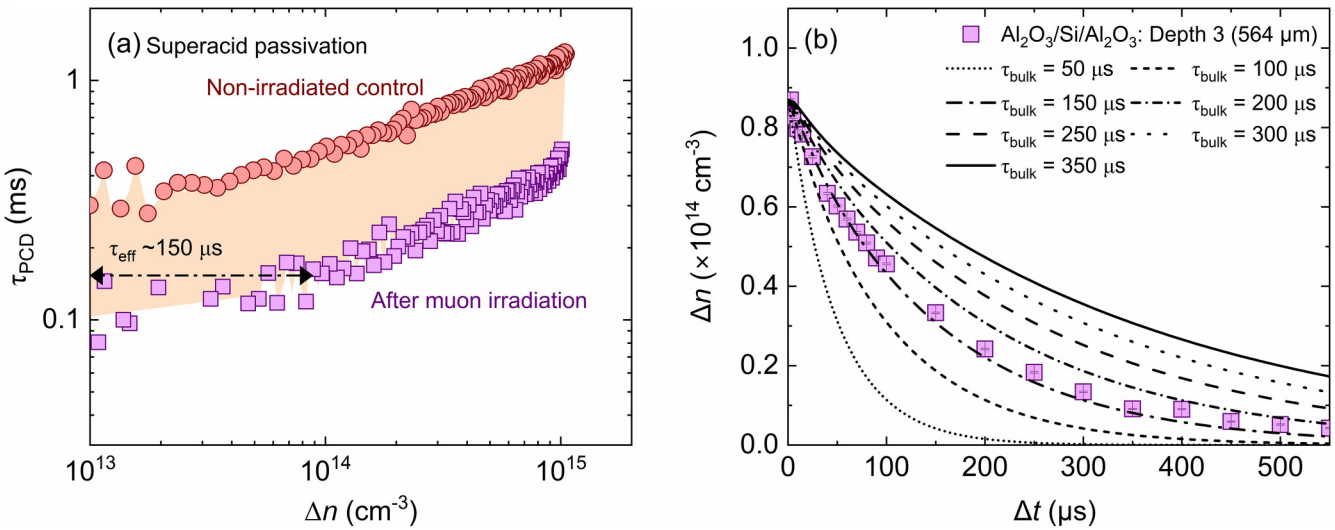

FIG. 3. (a) Injection-dependent PCD effective carrier lifetime for $Al_2O_3/Si/Al_2O_3$ following muon exposure and subsequent superacid passivation. Data for an identical superacid-passivated substrate without muon exposure are also shown. (b) Experimental photo-μSR CLS (purple squares) at Depth 3 (564 μm) with simulated curves for different bulk carrier lifetimes (50–350 μs). The SRV on both surfaces was fixed to 1 cm/s. The best fit in (b) is a 150 μs bulk carrier lifetime, also indicated in (a).

diffusion model, incorporating SRVs ranging from 1 to 10 000 cm/s on the muon-incident surface, and SRV fixed at ~1 cm/s [cf., Fig. 2(a)] on the Al_2O_3-passivated surface.

Figure 4 highlights significant variations in the carrier decay dynamics. $HfO_2/Si/Al_2O_3$ consistently exhibits the slowest decay across all depths, which indicates highly effective HfO_2 passivation. The slow decay at all depths suggests that recombination is largely bulk-limited or influenced by well-suppressed surface recombination at both surfaces. Good agreement with the simulated CLS is achieved with an SRV of ~50–100 cm/s at Depths 2 and 3, as shown in Figs. 2(b) and 2(c). This closely aligns with the ~42 cm/s upper-limit SRV extracted from the symmetrical $HfO_2/Si/HfO_2$ sample [cf., Fig. 2(a)], though we note that lower upper-limit SRVs (of order 10 cm/s) have been achieved for HfO_2 passivation on higher bulk carrier lifetime substrates.[23] For Depth 1 (HfO_2-passivated surface), the best agreement was for an SRV of ~1 cm/s. While this value is generally expected for HfO_2 passivation, this small discrepancy from Depths 2 and 3 falls within our modeling sensitivity limits.

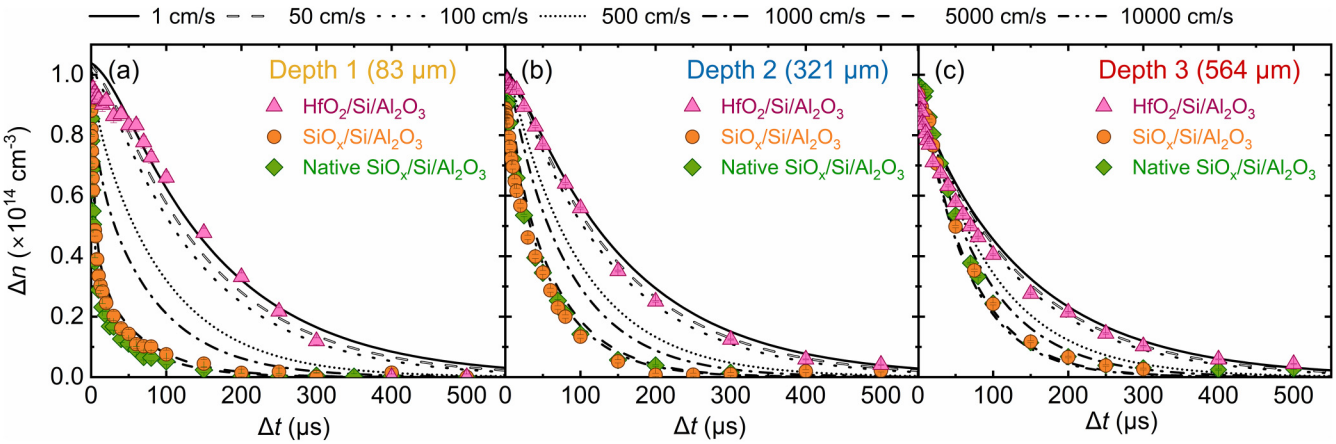

FIG. 4. Photo-μSR CLS for $HfO_2/Si/Al_2O_3$, $SiO_x/Si/Al_2O_3$, and native $SiO_x/Si/Al_2O_3$ samples at (a) Depth 1, (b) Depth 2, and (c) Depth 3. Curves are from the 1D diffusion model with SRVs on the muon-incident surface varied from 1 to 10 000 cm/s, and the SRV on the laser-incident surface (Al_2O_3-passivated) fixed at 1 cm/s in all cases.

Various mechanisms could contribute to differences in the values measured, including boron-oxygen defect activation under illumination,[27] and time-evolving bulk carrier lifetime changes from muon exposure. In $HfO_2/Si/Al_2O_3$ case, Depths 3, 1, and 2 were measured in sequence. Given that Depth 1 was measured after Depth 3, it may suffer from more muon-induced degradation, potentially altering τ_{bulk}. Degradation-related effects are less pronounced in poorly passivated samples, where surface recombination dominates. Furthermore, the fixed SRV of 1 cm/s on the Al_2O_3-passivated surface in all simulations may not perfectly match experimental conditions, e.g., due to sample-to-sample variation or minor handling damage.

In contrast to the effective passivation observed in $HfO_2/Si/Al_2O_3$, both $SiO_x/Si/Al_2O_3$ and native $SiO_x/Si/Al_2O_3$ exhibit rapid carrier decay due to poor passivation on the muon-incident surface, particularly at Depth 1 with SRVs of $\sim 10^4$ cm/s. The best agreement between model and experiment for these samples was obtained for muon-side SRVs approaching $\sim 10^4$ cm/s, consistent with those observed in symmetrical PCD samples [Fig. 2(a)]. At Depth 3, where carriers are generated closer to the Al_2O_3-passivated surface, the decay is slower, reinforcing the effect of asymmetry in surface passivation levels.

Native $SiO_x/Si/Al_2O_3$ showed the fastest decay of all three structures, particularly at Depth 1, suggesting extremely low passivation by the native oxide layer, with SRV likely exceeding 10^4 cm/s. Due to the model's limited sensitivity for high SRVs, simulated CLS curves for 5000 and 10 000 cm/s are nearly indistinguishable. Consequently, resolving differences between $SiO_x/Si/Al_2O_3$ and native $SiO_x/Si/Al_2O_3$ becomes challenging, although experimental data at Depth 1 suggest that SiO_x may offer marginally better passivation than "native SiO_x."

To compare the photo-μSR data with τ_{PCD} measured from the variable passivation surface, we extracted differential lifetimes ($\tau_{differential}$) from the measured photo-μSR CLS using[9]

$$\tau_{differential} = -\frac{\Delta n_{average}}{\left(\frac{\Delta(\Delta n)}{\Delta(\Delta t)}\right)}, \quad (5)$$

where $\Delta n_{average}$ represents the average of the two adjacent Δn values, $\Delta(\Delta n)$ is the difference between two adjacent Δn values, and $\Delta(\Delta t)$ is the corresponding time interval. We applied Eq. (5) to the CLS for the asymmetrically passivated samples as shown in Fig. 5 for Depth 1 (83 μm). For $HfO_2/Si/Al_2O_3$, $\tau_{differential}$ closely follows τ_{PCD}, confirming that differential lifetimes from photo-μSR reliably reproduce PCD lifetimes when SRV is low (~10–100 cm/s). By combining depth-resolved photo-μSR with differential lifetime analysis, one can, therefore, distinguish bulk- and surface-limited regimes. In contrast, for $SiO_x/Si/Al_2O_3$ and native $SiO_x/Si/Al_2O_3$, $\tau_{differential}$ is significantly lower compared to τ_{PCD} at $\Delta n = 1 \times 10^{14}$ cm^{-3}. It is only at lower injection levels ($\sim 2 \times 10^{13}$ cm^{-3}) that $\tau_{differential}$ begins to exceed τ_{PCD} due to rapid carrier recombination at the poorly passivated muon-incident surface (SRVs $\sim 10^4$ cm/s). Consequently, $\tau_{differential}$ values from photo-μSR are surface-dominated, whereas PCD measurements

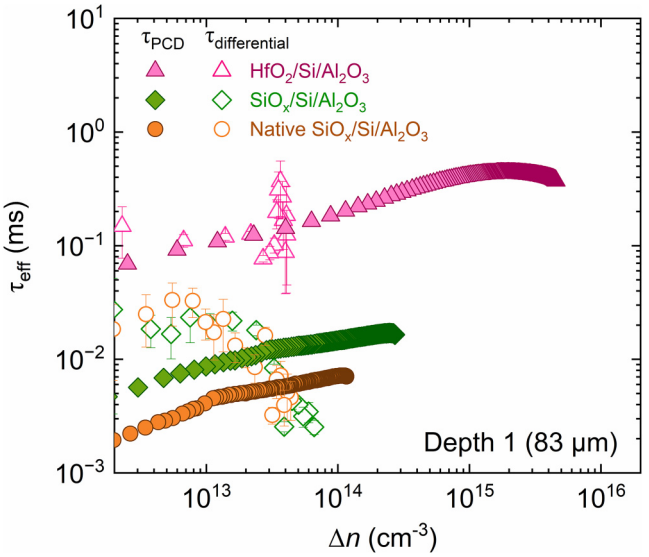

FIG. 5. Effective carrier lifetime (τ_{eff}) vs excess carrier density (Δn) for $HfO_2/Si/Al_2O_3$, $SiO_x/Si/Al_2O_3$, and native $SiO_x/Si/Al_2O_3$. Solid markers show τ_{PCD} with illumination from the variable passivation surface taken prior to muon irradiation. Open markers show $\tau_{differential}$ extracted from photo-μSR data at Depth 1 using Eq. (5). Error bars are based on propagation of Δn uncertainty into $\tau_{differential}$.

average carrier lifetimes over the entire wafer thickness and reflect the bulk-limited τ_{PCD} values.

IV. CONCLUSIONS

Photo-μSR, combined with a 1D diffusion model, is a sensitive technique for quantifying SRVs in passivated silicon wafers. By probing CLS at three implantation depths, photo-μSR can distinguish between bulk- and surface-limited recombination regimes, with strong agreement observed between modeled and experimental CLS for SRVs ranging ~10–5000 cm/s. The method works particularly well for structures with poor passivation (i.e., $SiO_x/Si/Al_2O_3$ and native $SiO_x/Si/Al_2O_3$). For improved accuracy, modeling approaches that account for bulk carrier lifetime changes could be deployed. Looking beyond silicon, photo-μSR holds promise for studying recombination in semiconductors, such as silicon carbide (SiC) and gallium arsenide (GaAs),[28] materials critical for advanced electronic and optoelectronic applications.

ACKNOWLEDGMENTS

We acknowledge muon beam time at the Science and Technology Facilities Council (STFC) ISIS Facility (Experiment No. RB2410172). The research was supported by EPSRC (Grant No. EP/V037749/1) and the Leverhulme Trust (Grant No. RPG-2020-377). A.Y. was supported by an ISIS Facility Development Studentship from the STFC and L.W. by an EPSRC Doctoral Training Partnership studentship (No. EP/W524645/1). S.L.P. was supported by a Royal Academy of Engineering Research Fellowship (No. RF-2324-23-197). The authors acknowledge use of the ALD facilities

within the Nano Fabrication Research Technology Platform at the University of Warwick.

AUTHOR DECLARATIONS

Conflict of Interest

The authors have no conflicts to disclose.

Author Contributions

Anup Yadav: Conceptualization (equal); Formal analysis (equal); Investigation (equal); Methodology (equal); Visualization (equal); Writing – original draft (equal). **Sophie L. Pain:** Conceptualization (equal); Formal analysis (supporting); Funding acquisition (supporting); Investigation (equal); Methodology (supporting); Visualization (supporting); Writing – review & editing (lead). **Luke Wilkins:** Investigation (supporting). **Nicholas E. Grant:** Conceptualization (equal); Methodology (supporting); Supervision (supporting); Writing – review & editing (supporting). **James S. Lord:** Investigation (supporting); Writing – review & editing (supporting). **Koji Yokoyama:** Conceptualization (equal); Funding acquisition (equal); Methodology (equal); Supervision (equal); Writing – review & editing (supporting). **John D. Murphy:** Conceptualization (equal); Funding acquisition (equal); Project administration (equal); Resources (equal); Supervision (equal); Writing – review & editing (equal).

DATA AVAILABILITY

The muon data that support the findings of this study are openly available in *ISIS Neutron and Muon Source Data Journal*, Ref. 29. Data underpinning figures in this article can be downloaded from https://wrap.warwick.ac.uk/193377/. The data that support the findings of this study are available from the corresponding author upon reasonable request. For the purpose of open access, the authors have applied a Creative Commons Attribution (CC BY) license to any Author Accepted Manuscript version arising from this submission.

REFERENCES

[1]A. B. Sproul, J. Appl. Phys. **76**, 2851 (1994).
[2]K. Yokoyama, J. S. Lord, J. Miao, P. Murahari, and A. J. Drew, Phys. Rev. Lett. **119**, 226601 (2017).
[3]R. F. Kiefl and T. L. Estle, *Semiconductors and Semimetals* (Elsevier, 1991), Vol. 34, p. 547.
[4]R. Kadono, A. Matsushita, R. M. Macrae, K. Nishiyama, and K. Nagamine, Phys. Rev. Lett. **73**, 2724 (1994).
[5]S. F. J. Cox, Rep. Prog. Phys. **72**, 116501 (2009).
[6]I. Fan, K. H. Chow, B. Hitti, R. Scheuermann, W. A. MacFarlane, A. I. Mansour, B. E. Schultz, M. Egilmez, J. Jung, and R. L. Lichti, Phys. Rev. B **77**, 035203 (2008).
[7]T. Prokscha, K. H. Chow, Z. Salman, E. Stilp, and A. Suter, Phys. Rev. Appl. **14**, 014098 (2020).
[8]K. Yokoyama, J. S. Lord, J. Miao, P. Murahari, and A. J. Drew, Appl. Phys. Lett. **118**, 252105 (2021).
[9]J. D. Murphy, N. E. Grant, S. L. Pain, T. Niewelt, A. Wratten, E. Khorani, V. P. Markevich, A. R. Peaker, P. P. Altermatt, J. S. Lord, and K. Yokoyama, J. Appl. Phys. **132**, 065704 (2022).
[10]A. Yadav, T. Niewelt, S. L. Pain, N. E. Grant, J. S. Lord, K. Yokoyama, and J. D. Murphy, J. Appl. Phys. **136**, 055707 (2024).
[11]N. E. Grant, T. Niewelt, N. R. Wilson, E. C. Wheeler-Jones, J. Bullock, M. Al-Amin, M. C. Schubert, A. C. van Veen, A. Javey, and J. D. Murphy, IEEE J. Photovoltaics **7**, 1574 (2017).
[12]R. W. Johnson, A. Hultqvist, and S. F. Bent, Mater. Today **17**, 236 (2014).
[13]S. L. Pain, L. Wilkins, A. Yadav, Y. Han, R. Beanland, N. E. Grant, and J. D. Murphy, Sol. Energy Mater. Sol. Cells **282**, 113439 (2025).
[14]N. E. Grant, A. I. Pointon, R. Jefferies, D. Hiller, Y. Han, R. Beanland, M. Walker, and J. D. Murphy, Nanoscale **12**, 17332 (2020).
[15]N. E. Grant, S. L. Pain, E. Khorani, R. Jefferies, A. Wratten, S. McNab, D. Walker, Y. Han, R. Beanland, R. Bonilla, and J. D. Murphy, Appl. Surf. Sci. **645**, 158786 (2024).
[16]A. Wratten, S. L. Pain, D. Walker, A. B. Renz, E. Khorani, T. Niewelt, N. E. Grant, and J. D. Murphy, IEEE J. Photovoltaics **13**, 40 (2023).
[17]N. E. Grant, S. L. Pain, J. T. White, M. Walker, I. Prokes, and J. D. Murphy, ACS Appl. Energy Mater. **5**, 1542 (2022).
[18]J. S. Lord, I. McKenzie, P. J. Baker, S. J. Blundell, S. P. Cottrell, S. R. Giblin, J. Good, A. D. Hillier, B. H. Holsman, P. J. C. King, T. Lancaster, R. Mitchell, J. B. Nightingale, M. Owczarkowski, S. Poli, F. L. Pratt, N. J. Rhodes, R. Scheuermann, and Z. Salman, Rev. Sci. Instrum. **82**, 073904 (2011).
[19]S. J. Blundell, R. De Renzi, T. Lancaster, and F. L. Pratt, *Muon Spectroscopy: An Introduction* (Oxford University Press, 2022).
[20]M. A. Green and M. J. Keevers, Prog. Photovoltaics **3**, 189 (1995).
[21]K. Sedlak, R. Scheuermann, T. Shiroka, A. Stoykov, A. R. Raselli, and A. Amato, Phys. Procedia **30**, 61 (2012).
[22]T. Niewelt, B. Steinhauser, A. Richter, B. A. Veith-Wolf, A. Fell, B. Hammann, N. E. Grant, L. Black, J. Tan, A. Youssef, J. D. Murphy, J. Schmidt, M. C. Schubert, and S. W. Glunz, Sol. Energy Mater. Sol. Cells **235**, 111467 (2022).
[23]S. L. Pain, E. Khorani, A. Yadav, T. Niewelt, A. Leimenstoll, B. F. M. Healy, M. Walker, D. Walker, N. E. Grant, and J. D. Murphy, RSC Appl. Interfaces **1**, 471 (2024).
[24]D. A. Neamen, *Semiconductor Physics and Devices* (McGraw-Hill Higher Education, New York, 2011).
[25]D. A. Clugston and P. A. Basore, in *Conference Record of the Twenty Sixth IEEE Photovoltaic Specialists Conference* (IEEE, 1997), p. 207.
[26]A. I. Pointon, N. E. Grant, E. C. Wheeler-Jones, P. P. Altermatt, and J. D. Murphy, Sol. Energy Mater. Sol. Cells **183**, 164 (2018).
[27]D. Macdonald, F. E. Rougieux, A. Cuevas, B. Lim, J. Schmidt, M. Di Sabatino, and L. J. Geerligs, J. Appl. Phys. **105**, 093704 (2009).
[28]K. Yokoyama, J. S. Lord, P. W. Mengyan, M. R. Goeks, and R. L. Lichti, Phys. Rev. Res. **6**, 033140 (2024).
[29]S. Pain, K. Yokoyama, N. Grant, T. Niewelt, A. Yadav, J. Murphy, and J. Lord, "Establishing the limitations of photoexcited muon spin spectroscopy," in *ISIS Neutron and Muon Source Data Journal* (STFC, 2024).